JES Focus Issue on Advances in Modern Polymer Electrolyte Fuel Cells in Honor of Shimshon Gottesfeld

Nanofiber Fuel Cell MEAs with a PtCo/C Cathode

J. J. Slack,[1] C. Gumeci,[2] N. Dale,[2] J. Parrondo,[2] N. Macauley,[3] R. Mukundan,[3,*] D. Cullen,[4] B. Sneed,[4] K. More,[4] and P. N. Pintauro[1,*,z]

[1]*Department of Chemical and Biomolecular Engineering, Vanderbilt University, Nashville, Tennessee 37235, USA*
[2]*Nissan Technical Center North America, Farmington Hills, Michigan 48331, USA*
[3]*Los Alamos National Laboratory, Los Alamos, New Mexico 87545, USA*
[4]*Center for Nanophase Material Sciences, Oak Ridge National Laboratory, Oak Ridge, Tennessee 37831, USA*

PtCo/C and Pt/C catalyst powders were incorporated into electrospun nanofiber and conventional sprayed cathode membrane-electrode-assemblies (MEAs) at a fixed electrode loading of 0.1 mg_{Pt}/cm^2. The binder for PtCo/C nanofiber cathodes and Pt/C nanofiber anodes was a mixture of Nafion and poly(acrylic acid) (PAA), whereas the sprayed electrode MEAs utilized a neat Nafion binder. The structure of electrospun fibers was analyzed by scanning transmission electron microscopy (STEM) and energy-dispersive X-ray spectroscopy (EDS), which showed that the fibers were ~30% porous with a uniform distribution of catalyst and binder in the axial and radial fiber directions. The initial performance of nanofiber MEAs at 80°C was 20% better than the sprayed electrode MEA (a maximum power density of 1,045 mW/cm^2 vs. 869 mW/cm^2). The benefit of the nanofiber electrode morphology was most evident at end-of-test (after a metal dissolution accelerated stress test), where power densities dropped by only 8%, after 30,000 square wave voltage cycles (0.6 V to 0.95 V), as compared to a 35% drop in the maximum power for the sprayed electrode MEA. The use of a recovery protocol improved the initial performance of a nanofiber MEA by ~13%, to 1,070 mW/cm^2 at 0.65 V, and increased the power after a metal dissolution stress test by 5–10% (e.g. 840 mW/cm^2 at 0.65 V after 30,000 voltage cycles). At rated power, the nanofiber MEA generated more than 1,000 mW/cm^2 at 99°C and a pressure of 250 $kPa_{abs.}$ The high performance and durability of PtCo/C nanofiber cathode MEAs is due to the combined effects of a highly active cathode catalyst and the unique nanofiber electrode morphology, where there is a uniform distribution of catalyst and binder (no agglomeration) and short transport pathways across the submicron diameter fibers (which lowers gas transfer resistance and facilitates water removal from the cathode).
 [DOI: 10.1149/2.0151907jes]

Manuscript submitted January 3, 2019; revised manuscript received March 12, 2019. Published April 22, 2019. *This paper is part of the JES Focus Issue on Advances in Modern Polymer Electrolyte Fuel Cells in Honor of Shimshon Gottesfeld.*

The hydrogen/air proton-exchange membrane fuel cell (PEMFC) is a promising energy conversion device for automotive applications due to its high power output, high-energy conversion efficiencies and moderate operating temperature,[1,2] but the high cost and poor durability of Pt-based catalyst electrodes are issues that require further attention and improvement. In 2011, Zhang and Pintauro showed that a particle/polymer fiber mat cathode, made by nanofiber electrospinning a mixture of Pt/C powder, Nafion and poly(acrylic acid) (PAA), out-performed a conventional slurry cathode in initial H_2/air fuel cell tests, where high power was produced at a low Pt loading.[3] In three following-on papers, Brodt et al.[4–6] extended this initial work by: (i) demonstrating that the fiber structure/performance was robust, with high power generation for fiber mat cathodes of different catalyst/binder ratios and different fiber diameters, (b) showing improved cathode durability as compared to a conventional slurry electrode design after a carbon corrosion voltage cycling accelerated test, and (c) identifying a new cathode binder (a mixture of Nafion and polyvinylidene fluoride) which lowered the rate of carbon corrosion with significantly higher power densities after an accelerated voltage cycling carbon corrosion test, as compared to a nanofiber cathode MEA with a Nafion/PAA binder or a slurry electrode MEA with neat Nafion binder.

There have been numerous advances in new Pt-alloy powder catalyst for the cathodic oxygen reduction reaction in a H_2/air proton exchange membrane fuel cell,[7–11] including alloy materials (e.g., PtCo and PtNi on carbon) and new catalyst morphologies (e.g., core-shell catalysts). A logical next step in the development/analysis of nanofiber fuel cell MEAs is to examine such catalysts to: (a) identify conditions for electrospinning submicron diameter particle/polymer fibers with a high particle loading and a Nafion-based binder, (b) analyze the structure of the resulting fibers, and (c) evaluate the performance and durability of the resulting MEAs in a PEM fuel cell.

In the present study, a commercial PtCo/C catalyst (46.7 wt% Pt, 5.4 wt% Co, 47.9 wt% C), supplied by Tanaka Kikinzoku Kogyo (TKK), was incorporated into nanofiber cathode MEAs using a Nafion/poly(acrylic acid) (PAA) cathode binder. The performance and durability of these MEAs were assessed in a H_2/air fuel cell at a cathode catalyst loading of 0.1 mg_{Pt}/cm^2. PtCo/C and Pt/C (with 40 wt% Pt) cathode catalyst MEAs were compared at the same total Pt loading, without correcting for small differences in electrode thickness and possible differences in fiber morphology. The PtCo/C nanofiber cathode MEAs were compared to spray cathode MEAs with the same catalyst where the binder was neat Nafion and to a nanofiber cathode MEA with Pt/C catalyst from Johnson Matthey.

Experimental

Electrode preparation.—Electrospinning inks were prepared using a carbon supported catalyst, a Nafion dispersion (Liquion 1115 1100 EW) and 450 kDa poly(acrylic acid) (Sigma Aldrich) as the electrospinning carrier polymer. The catalyst powder was either 52 wt% PtCo on porous carbon (TKK TEC36E52) or 40 wt% Pt/Vulcan carbon (Johnson Matthey HiSPEC 4000). Inks were made with an isopropyl alcohol/water solvent. The solids content of the inks for nanofiber electrodes was 15 wt%, much higher than the solids content for spray electrode inks (4.6 wt%).[4] Spray inks have a low viscosity to achieve uniform catalyst distribution by atomization[12] whereas a high viscosity ink with sufficient polymer chain entanglements is required for fiber formation during electrospinning.[3] All electrospinning inks were prepared using the following sequence of steps: (1) catalyst powder was added to water and sonicated for 30 minutes in an ice bath (2) Nafion solution was added followed by an additional 30 minutes of ice bath sonication and (3) poly(acrylic acid) (PAA) was added and the mixture was mechanically stirred for two days.

Electrospinning was carried out using a single stainless steel 22 gauge needle-tipped syringe as the spinneret, with a rotating and horizontally oscillating drum collector, as described in References 3–6. Nanofiber mats were electrospun by controlling the voltage bias between the needle tip and the grounded drum collector, the ink flow rate, relative humidity, and distance from needle tip to collection drum. The

*Electrochemical Society Fellow.
[z]E-mail: peter.pintauro@vanderbilt.edu

final platinum loading of the electrode was controlled by the duration of the electrospinning process. The conditions to electrospin fibers with catalyst powder (Pt/C or PtCo/C), Nafion, and PAA were: 12 kV, 0.75 mL/hr, 40% RH, and 8 cm from tip to collector. The PtCo/C dry mat composition for nanofiber mat cathodes was 65/23/12 catalyst/Nafion/PAA, which correlates to an ionomer to carbon (I/C) ratio of 1.1 where the ionomer in this case is defined as the sum of Nafion and PAA. Nanofiber anodes contained Johnson Matthey 40% Pt/C on HiSPEC 4000 catalyst with the same catalyst/Nafion/PAA wt. ratio as the PtCo/C cathodes.

Spray inks were prepared at Nissan Technical Center of North America (NTCNA). Typically, the catalyst inks were made by mixing water and n-proponal with a Nafion ionomer dispersion (20 wt%). The mass-based ionomer/carbon (I/C) ratio in the ink was kept constant at 1.1 and the water/alcohol weight ratio was 1/1. The ink was well-mixed using a homogenizer (Ika T25) for 4 hours. An electrocatalyst layer was sprayed onto a gas diffusion layer (Sigracet 29 BC GDL) using an automated robotic spray system (Asymtek, Nordson). The spray electrodes from NTCNA also had a layer of Nafion sprayed onto their surface (at 0.5 mg_{Nafion}/cm^2) prior to hot-pressing to improve electrode/membrane attachment. No such sprayed layer was used with nanofiber mat electrodes.

Membrane-electrode-assembly (MEA) preparation.—A series of nanofiber and spray MEAs were prepared. The anode and cathode Pt loadings for all nanofiber MEAs were each 0.1 $mg_{Pt}/cm^2 \pm 0.01$ mg_{Pt}/cm^2. This 10% error in the loading measurement is propagated into any values that use loading in their calculation (e.g. mass activity and ECSA). MEAs with a nanofiber cathode also had a nanofiber anode. As-spun nanofiber anode and cathode mats were simultaneously hot pressed directly onto a NR211 membrane at 140°C and 4 MPa for 5 minutes. For anode/cathode spray electrode MEAs, the binder was neat Nafion (no PAA) at a catalyst/Nafion weight ratio of 65/35. Spray cathode loading was ∼0.1 mg_{Pt}/cm^2 and sprayed anode loading was 0.4 mg_{Pt}/cm^2, resulting in a total MEA loading of ∼0.5 mg/cm^2. The sprayed anode loading above 0.1 mg/cm^2 does not affect performance. All nanofiber and sprayed MEAs were prepared using a Nafion NR211 membrane and Sigracet 29 BC gas diffusion layers (GDLs).

Nanofiber MEAs were prepared at Vanderbilt University by hot pressing at 2 MPa and 140°C for 5 minutes. Sprayed electrode MEAs were prepared at NTCNA by hot pressing gas diffusion electrodes with 2 MPa at 130°C for 10 minutes. There was no attempt to optimize the hot-pressing conditions for either type of MEA.

Structural characterization of electrospun nanofibers.—Nanofiber mats were imaged using a Zeiss Merlin scanning electron microscope (SEM) at the Vanderbilt Institute of Nanoscale Science and Engineering, with an accelerating voltage of 10 kV (as was used in the past to analyze this type of sample)[3] and a working distance of 8 mm. Scanning transmission electron microscopy (STEM) tomography was performed using a 200kV FEI Talos F200X STEM at Oak Ridge National Laboratory with a Gatan High Tilt tomography holder for FEI instruments. The holder was plasma-cleaned for 5 minutes prior to use, after which the sample was loaded and a 20 minute ozone cleaning treatment (10 minutes/side) was used to reduce possible hydrocarbon deposition (contamination). Bright field (BF) and high angle annular dark field (HAADF) image pairs (1024 by 1024 pixels) were acquired in 5° tilt increments over a tilt range of ±75° (150° total). This results in a series of STEM images referred to as a "tilt series". Tilt series alignment and tilt-axis corrections were performed manually for each image stack using computer software (Fiji/ImageJ and Tomviz (tomviz.org)). A 3D reconstruction of a 2 micron length of a single nanofiber was performed for the bright field tilt series using a bright-field model-based iterative reconstruction algorithm (MBIR) which accounts for diffraction contrast

MEA characterization and testing in fuel cell.—Nanofiber and spray electrode MEAs were evaluated at Vanderbilt University (5 cm^2 MEA with a single serpentine flow channel test fixture with H_2/air flow rates of 125/500 sccm), Nissan Technical Center North America (a 10 cm^2 MEA with parallel feed gas flow channels with H_2/air flow rates of 4000/8000 sccm), and Los Alamos National Laboratory (5 cm^2 MEA differential cell with H_2/air flow rates of 500/2000 sccm). Hydrogen/air fuel cell polarization data were collected at 80°C, 200 kPa absolute pressure and either 100% relative humidity (RH) or 40% RH.

Oxygen reduction reaction mass activity was obtained using methodologies in the literature[13] at 80°C and 0.9 V with fully humidified hydrogen/oxygen at 150 kPa absolute pressure and anode and cathode flow rates of 100/100 sccm H_2/O_2. The electrochemical surface area (ECSA) of cathodes was determined from cyclic voltammograms of H_2 generation/stripping with stagnant H_2 gas at ambient pressure and 30°C.[14] The estimated error in ECSA and mass activity is 10%, a consequence of the 10% uncertainty in determining the Pt loading of a cathode.

Oxygen gas transport resistance (GTR, with units of s/m) including Knudsen diffusion resistance and transport resistance through the ionomer and liquid water, was used as a characteristic measure of reactant gas (oxygen) diffusivity in the catalyst layer. The O_2 GTR was estimated by separating molecular diffusion resistance from the total gas transport resistance by measuring the limiting current at various oxygen concentrations and pressures[15] under the following experimental conditions: an anode (H_2) flow rate of 4000 sccm, a cathode gas flow rate of 8000 sccm (O_2 with N_2), a pressure of 100, 150, 200, and 250 kPa (abs), and 80°C. Limiting currents were obtained by linear sweep voltammetry using an external potentiostat in the potential window of 0.1 V–0.95 V at a scan rate of 10 mV/s for 4 cycles. Experiments were conducted with five different cathode feed gas oxygen concentrations: 0.000%, 0.525%, 0.787%, 1.838% and 2.625% O_2, where the balance was nitrogen (the O_2/N_2 composition was set by mass flow controllers). The gases were supplied at a high flow rate to minimize the in-plane reactant gas concentration differential. The relative humidity (RH) of inlet gases (O_2/N_2 mixtures and H_2) was set at 90%, as has been done in previous studies;[16–18] thus at 100% RH conditions, there was a decrease in the limiting current due to flooding whereas at low RH conditions (∼70%), the limiting current was not clearly observable due to a high IR drop across the membrane and the catalyst layer.

Electrochemical impedance spectroscopy (EIS) measurements were performed in H_2/N_2 mode to determine proton transport resistance in the catalyst layer (also referred to as ionomer resistance) and in H_2/air and HelOx to quantify kinetic and mass transport losses. The H_2/N_2 EIS measurements were carried out using a 10 cm^2 cell and an an Autolab potentiostat in a four-electrode configuration at 80°C in the frequency range 15,000 Hz to 0.1 Hz with an AC amplitude of 10 mV. The applied voltage (DC) was kept at 0.45 V. Measurements were taken at 100 frequencies logarithmically spaced using a single sine wave type function, after equilibrating the cell for at least 30 to 60 minutes. The fuel cell was supplied with H_2 at the anode and N_2 at the cathode, each at a flow rate of 500 sccm and RH was fixed at 100% for both electrodes. Proton transport resistance is deduced from Nyquist plots obtained using EIS; this measurement of proton transport resistance is detailed in References 19–21. EIS measurements in H_2/air and HelOx were performed to quantify kinetic and mass transport losses on 5 cm^2 differential cells at 0.2 and 2.0 A/cm^2. The cell temperature was 80°C, with 1000 sccm of H_2 and 3000 sccm of air supplied to the anode and cathode at 100%RH and 150kPa outlet pressure. The AC current amplitude for the EIS was ±5% of the applied DC current and the frequency was swept from 10kHz to 0.1Hz with 12 points collected per decade.

A standard metal dissolution accelerated stress test[22] (AST) was performed with H_2 (anode) and N_2 (cathode) feed gases at 80°C and 100% RH. A square wave voltage cycling regimen (3 seconds at 0.60 V and 3 seconds at 0.95 V) was repeated 30,000 times using an external potentiostat. Fuel cell voltage-current polarization data, mass activity, ECSA, and GTR were measured before and after the AST. As is standard procedure, mass activity and ECSA after the AST were calculated using the initial cathode Pt loading.[5,6]

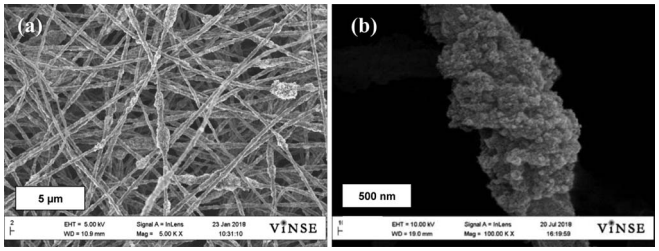

Figure 1. SEM images of nanofiber mat with a binder of Nafion/PAA containing PtCo/C at (a) (5000x), and (b) PtCo/C (100,000x).

Both nanofiber and sprayed cathode MEAs were subjected to additional testing at Los Alamos National Lab in a 5 cm^2 differential cell following the procedure reported by Baker et al.[15] MEAs were subjected to a recovery protocol[23] several times in order to maximize mass activity and fuel cell performance and to eliminate the role of recoverable losses during catalyst ageing studies. The recovery protocol was applied four times after conditioning (break-in) in order to achieve a maximum initial performance and then to recover the performance after 15,000 and 30,000 square wave (0.6 V and 0.95 V for 3.0 s each) accelerated stress test (AST) cycles. The specific recovery protocol consisted of a 1.0 hour hold at 0.4V in H_2/air with the cell at T = 35°C and the humidifier bottles at T = 40°C, which allows for a substantial amount of water to wash out impurities from the cathode catalyst. Next, a H_2 pumping current was applied for 1.0 hour with a H_2/N_2 feed gases, resulting in a zero or mildly negative voltage to desorb impurities from the cathode catalyst surface.

Results and Discussion

PtCo/C nanofiber structure.—Figures 1a and 1b show scanning electron micrographs of a (PtCo/C)/Nafion/PAA fiber mat and an individual electrospun fiber, respectively. The surface of the fibers is uniformly roughened (Figure 1b) due to the high catalyst particle content and there are no large electro-spray droplets in Figure 1a. The average diameter of the fibers is approximately 600 nm, as determined by ImageJ analysis of digitized micrographs. These images are similar to those previously published for Pt/C catalyst with Nafion/PAA binder.[3–5] Figure 2 shows STEM images of a 2 µm length of electrospun fiber. The STEM dark field image of the nanofiber during the tilt-series is shown in Figure 2a, the length-wise fiber cross section generated from these images is shown in Figure 2b and the resultant reconstruction is shown in Figure 2c. The results show a uniform distribution of catalyst and binder along the fiber length. The computed fiber porosity was 31%. The distribution of Pt and F (i.e., Nafion binder) determined by EDS along a fiber cross-section and in a fiber segment are shown in Figures 3a and 3b (elemental maps) and Figure 3c (a line scan of Pt and F across a fiber).

Electrochemical characterization.—H_2/air fuel cell tests were carried out at 80°C, 200 kPa, and 100% RH. Figure 4 compares the performance of nanofiber MEAs with a PtCo/C cathode and a Johnson Matthey Pt/C cathode (from Reference 5). Measured current-voltage data and IR-corrected plots are shown. The lower performance of the Pt/C catalyst is due to its lower ORR activity, as compared to PtCo/C. The PtCo/C catalyst generated >30% higher power, as compared to Pt/C. The ECSA of PtCo/C and Pt/C nanofiber cathodes were nearly identical (48 vs. 45 m^2/g). The high power output with PtCo/C was associated with its significantly higher ORR mass activity; 270 mA/mg_{Pt} for PtCo/C which is ~70% greater than that of a Pt/C fiber cathode (160 mA/mg_{Pt}) and 2.5x greater than that of a Pt/C spray electrode with Nafion (110 mA/mg_{Pt}) from Reference 5.

Polarization data from PtCo/C cathode MEAs with a sprayed or nanofiber electrode morphology are shown in Figure 5 at beginning-of-life (BOL) and end-of-test (EOT), where the latter refers to MEA performance after 30,000 voltage cycles of a metal dissolution AST. The results in this figure were reproducible to within ± 5% and the data represent averages from multiple repeat experiments. It should be noted here that the sprayed MEA utilized neat Nafion as the binder (no PAA was needed, whereas PAA is critical for fiber formation via electrospinning) and the anode loading was higher than the nanofiber anode (0.4 vs. 0.1 mg/cm^2). Despite these differences, important findings can be drawn from Figure 5 and the associated measurements of ECSA, mass activity, ionomer resistance, and GTR (listed in Table I). The improved power densities of the nanofiber electrode MEA (1,045 vs. 869 mW/cm^2 for maximum power and 751 vs. 715 mW/cm^2 for the power density at 0.65 V) is associated with the combined effects of a higher mass activity and a lower GTR, a consequence of the high inter-fiber and intra-fiber porosity of the nanofiber cathode with little or no catalyst/binder agglomeration. The larger ECSA for nanofiber MEA cathodes results in a higher Pt roughness factor (the product

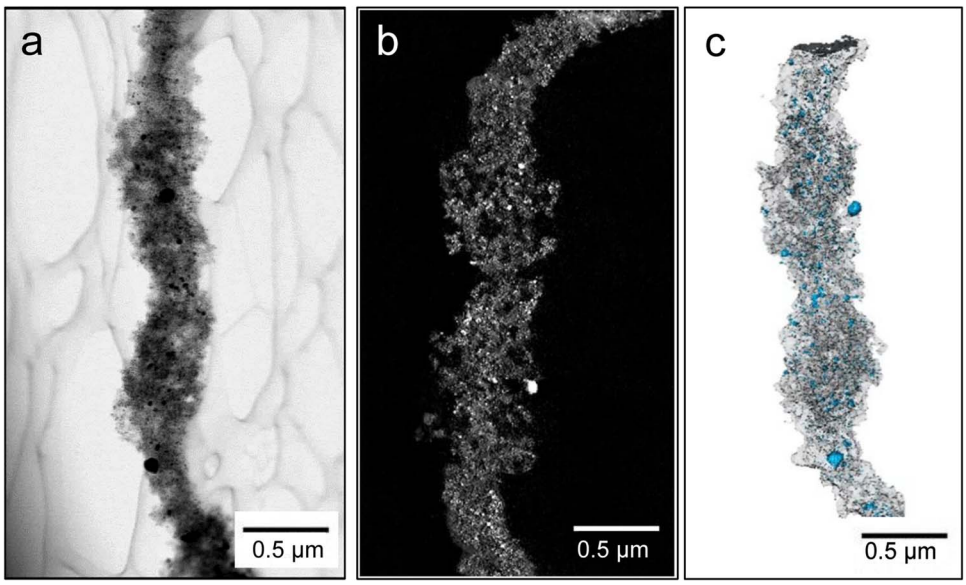

Figure 2. (a) The STEM-image of the 2 micron length of nanofiber at the beginning of the tilt series (75° from perpendicular) (b) The length-wise cross-section of the nanofiber generated from the 3D reconstruction. The bright spots are metal particles, the gray areas are Nafion, PAA, or carbon, and the black is void-space (c) the total 3D reconstruction showing PtCo particles in blue, Nafion/PAA/C in gray, and void space in white.

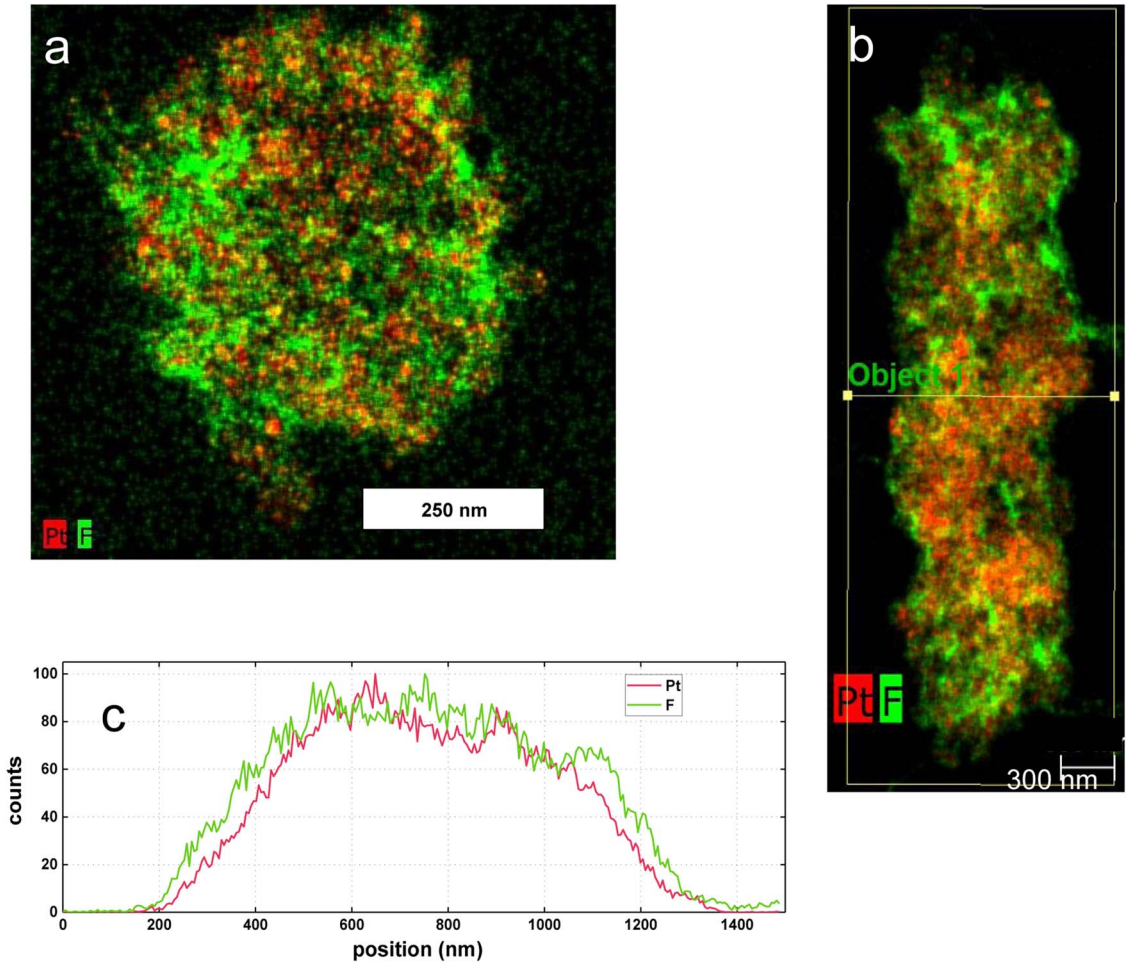

Figure 3. Fluorine and Pt signals from energy dispersive X-ray spectroscopy for (a) elemental map for a fiber cross-section, (b) elemental map along the length of the nanofiber and (c) the line scan distribution of Pt and F for the fiber cross-section shown in (b).

of ECSA and platinum loading), which has been shown to correlate inversely with gas transport resistance.[24] It is well established in the literature that gas transport resistance leads to significant voltage loss in the high current density region of the polarization curve especially for low Pt loading cathodes.[25,26] Thus, the lower GTR in nanofiber cathodes is consistent with the higher power densities at high current densities shown in Figure 5.

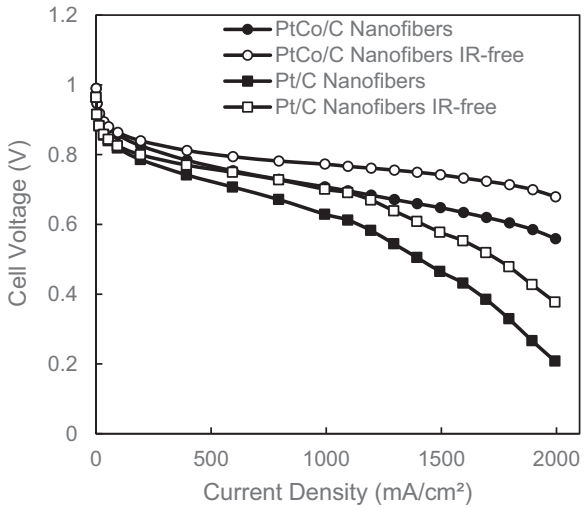

Figure 4. H_2/air fuel cell polarization data (IR-corrected and uncorrected) comparing two types of catalysts in nanofiber cathode MEAs (TKK PtCo/C and JM Pt/C[5]) at 100% RH, 80°C and 200 kPa absolute pressure.

The real distinction between a sprayed and nanofiber electrode MEA and the benefits of the nanofiber electrode morphology are seen at EOT. The spray electrode lost 32% of its maximum power after the metal dissolution AST, as compared to an 8% power loss for the nanofiber electrode MEA, with smaller losses in both ECSA and mass activity. In a previous study, Brodt et al.[5] showed that sprayed and nanofiber MEAs with Pt/C cathode catalyst exhibited similar durability after 10,000 metal dissolution voltage cycles.[5] The present results show that the two MEA morphologies diverge after extended voltage cycling. At EOT, the GTR of nanofiber cathodes was lower than that of a sprayed cathode at BOL. Thus, as compared to a conventional fuel cell electrode, nanofiber cathodes exhibited a lower initial resistance to oxygen and water vapor transport and retain these low resistances after a voltage cycling AST durability experiment. The low transport resistances are due to the unique mat morphology, with high inter and intra-fiber porosity, more accessible Pt sites (evident from the high ECSA) and a thinner (more uniform) ionomer coating on catalyst particles (no agglomerates), as compared to sprayed/conventional MEAs.

Table I includes the BOL and EOT ionomer resistance in the catalyst layer for both spray and nanofiber electrodes measured using H_2/N_2 EIS as described in the experimental section. These ionomer resistance values should not be confused with kinetic and mass transport resistance values obtained using H_2/air and HelOx EIS experiment (as shown in Figure 9). In general, ionomer resistance was lower

Table I. Electrochemically active surface area and mass activity of nanofiber and spray electrode MEAs at beginning and end of life (after 30,000 metal dissolution cycles).

	ECSA (m^2/g_{Pt})		Mass Activity (mA/mg_{Pt})		Gas Transport Resistance (GTR) (s/m)		Ionomer Resistance ($\Omega \cdot cm^2$)	
	BOL	EOT	BOL	EOT	BOL	EOT	BOL	EOT
PtCo/C Spray	44	33	190	144	52	68	0.19	0.29
PtCo/C Nanofibers	48	41	270	219	35	37	0.14	0.19

in the case of nanofiber electrodes, as compared to those of sprayed electrodes. This is attributed to a number of factors, including fewer catalyst sites poisoned by Nafion's sulfonic acid sites (lower Nafion content), and a more even distribution of catalyst and ionomer within the fiber network. The results are consistent with Subbaraman et al.,[27] who showed that Nafion is blocking the active sites of Pt catalysts, and the work of Shinozaki et al.[28] where it was shown that electrochemically active surface area and oxygen reduction activity decreased as the ionomer/carbon (I/C) ratio of a cathode catalyst layer increased.

To further explain the excellent durability of nanofiber MEAs after 30,000 metal dissolution voltage cycles, the size and composition of PtCo nanoparticles in the cathode layer before and after the AST were determined. Post-mortem analyses of sprayed and nanofiber cathodes were carried out at Oak Ridge National Laboratory using a combination of Scanning Transmission Electron Microscopy (STEM) and Energy-Dispersive X-ray Spectroscopy (EDS). The diameter of PtCo particles was obtained from STEM micrographs (High-Angle Annular Dark-Field images, such as that shown in Figure 6a), which were binarized using ImageJ software (Figure 6b). Approximately 200 nanoparticles were numbered, their size was measured, and their composition was determined by EDS. A comparison of the results (Co composition of nanoparticles vs. PtCo nanoparticle size at BOL and EOT) is shown in Figures 7a, 7b for a nanofiber and sprayed cathode.

The average percentage of cobalt retained in a nanoparticle within the nanofiber cathode was found to be 61% ± 4% while for the sprayed electrode, that average percentage of retained Co was 49% ± 5%. Better Co retention implies better Pt retention and is consistent with the observed higher power output at EOT for the nanofiber MEA, although it is not known if the Pt/Co ratio remains constant before/after a voltage cycling accelerated stress test. At EOT, the sprayed electrode showed greater particle growth at EOT due to Ostwald ripening and/or agglomeration.[29] Thus, the retention of power observed in the nanofiber MEA at EOT is in part due to the retention of cobalt in the PtCo nanoparticles (the catalytic enhancement effect of Co in PtCo is better retained) and less metal nanoparticle growth, with the assumption that there is also less Pt dissolution. The sprayed cathode results are qualitatively consistent with those of Myers et al.[30] who showed that the mass activity of PtCo/C catalyst dropped by approximately 50% and the particle size increased from ~4 nm to ~14 nm after 30,000 square wave voltage cycles in a metal dissolution AST.

Rated power.—The rated power of a hypothetical 90 kW fuel cell stack with nanofiber electrode MEAs containing a PtCo/C cathode was determined at various temperatures (80°C, 95°C, and 99°C) for an operating pressure of 150–250 kPa (absolute) and a total anode + cathode Pt loading of 0.2 mg/cm^2. The voltage at which rated power was measured was found using Equation 1 with Q/ΔT equal to 1.45 kW/°C.[31,32]

$$Q/\Delta T = \frac{[Stack\ Power(kW) \times (1.25 - V\ @rated\ power)/V\ @rated\ power]}{Cell\ Operating\ Temperature(^{\circ}C) - Ambient\ Temperature(^{\circ}C)} \quad [1]$$

Values of rated power are listed in Table II. At a total MEA Pt loading of 0.2 mg/cm^2, the rated power of 1,072 mW/cm^2 at 99°C and 250 kPa pressure translates into a total fuel cell stack Pt content of only 16.8 grams, which is quite reasonable and cost effective.

Recovery protocol.—The effect of the recovery protocol is illustrated in Figure 8 where the performance in both the kinetic and mass transport region improves significantly. Four repeated recovery cycles were sufficient to reach a maximum initial MEA performance. For example, the peak power at BOL increases from 1,050 to 1,140 mW/cm^2 at 200 kPa. After the recovery process the mass

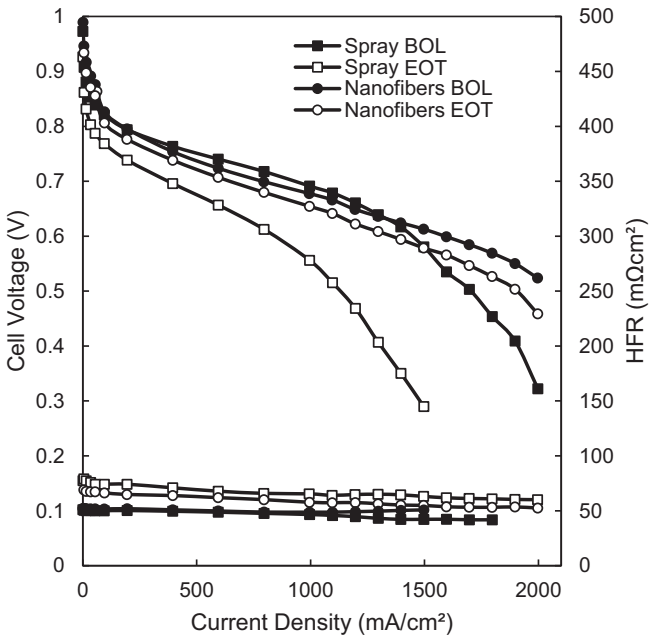

Figure 5. H_2/air fuel cell polarization data for nanofiber and sprayed electrode electrode MEAs using PtCo/C cathodes and Pt/C anodes at 80°C, 100% RH and 200 kPa absolute with feed gas flow rates of 4000/8000 sccm H_2/air. BOL data were collected after break-in. EOT data collected after 30,000 square-wave voltage cycles, 0.60 V to 0.95 V.

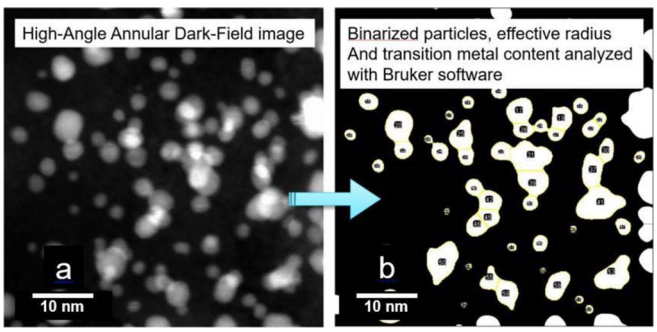

Figure 6. STEM image converted to a "binary" image that only contains white and black pixels such that imageJ can calculate an area for each particle. These metal nanoparticles of PtCo are within a sprayed electrode at EOT. Particle agglomeration is observed.

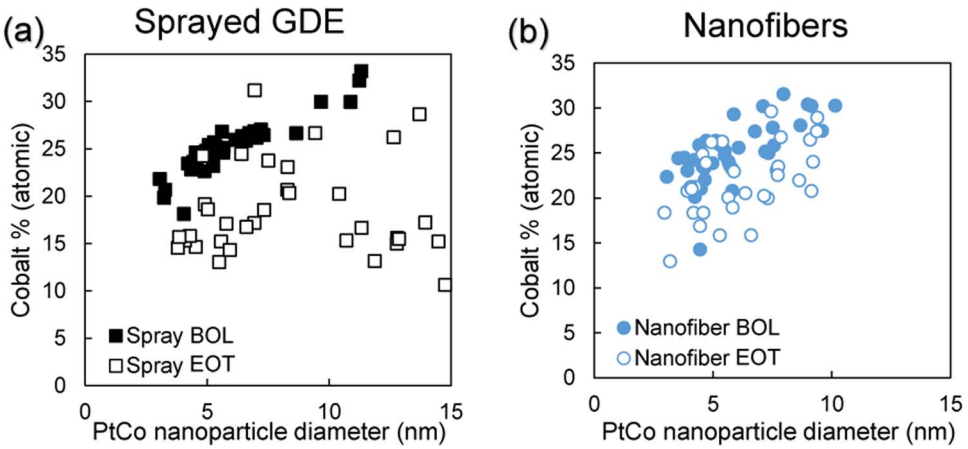

Figure 7. Cobalt content of individual nanoparticles with respect to the nanoparticle size for both NTCNA sprayed GDE and electrospun nanofiber electrode MEAs before and after metal dissolution AST.

activity of the nanofiber cathode MEA (based on the initial weight of catalyst) reaches a maximum of 464 mA/mg$_{pt}$ while the sprayed electrode reaches 431 mA/mg$_{Pt}$ (see Table III). The recovery process also improves the GTR at every stage of the AST with the recovered amount decreasing with catalyst ageing. The recovery protocol decreases the BOL nanofiber cathode GTR to 21 s/m (Table III) vs. 35 s/m shown in Table I. After 15,000 voltage cycles of AST the recovery protocol decreases the GTR from 35 to 28 s/m. After 30,000 metal dissolution voltage cycles and 4 recovery cycles, the GTR of the nanofiber cathode was 35 s/m while the spray cathode was 52 s/m, showing a much better retention of gas transport properties. These results illustrate the importance of the recovery protocol in evaluating the maximum performance achievable with any MEA. It should be noted that the recovered performance (polarization and mass activity) after 15,000 AST cycles is actually better than the BOL performance (mass activity of 496 mA/mg$_{Pt}$) illustrating that the initial loss in power is due to processes that are reversible. However, after 30,000 cycles, the performance (polarization, mass activity and GTR) are degraded from BOL due to irrecoverable voltage losses.

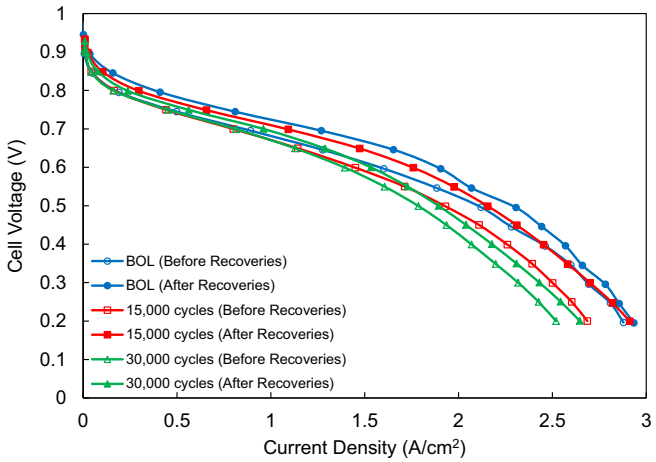

Figure 8. Polarization data for a 5 cm^2 nanofiber MEA with a PtCo/C cathode at 80°C, 100% RH, 200 kPa, with feed gas flow rates of 500 sccm H_2 at the anode and 2000 sccm at the cathode.

Electrochemical impedance spectroscopy (EIS).—EIS data were collected at LANL for cathode gas feeds of air and HelOx (21%O_2, Bal: Helium), in order to quantify kinetic and mass transport losses. Figure 9a illustrates the EIS spectra (1 Hz to 5000 Hz) obtained at a low current density (0.2 A/cm^2, representative of the kinetic region) and high current density data (2.0 A/cm^2, representative of the mass transport region) are shown in Figure 9b. The measured EIS data is represented by the filled (BOL) and open (30,000 cycles) symbols whereas the equivalent circuit fit is represented by the solid (BOL) and dashed (30,000 cycles) lines. A simple equivalent circuit model reported earlier[33] was used to fit the data and quantify a high frequency resistance (HFR) and kinetic and mass transport resistances. The HFR is constant throughout the experiment at a value of $\approx 0.055\ \Omega{\cdot}cm^2$ indicating no changes to the conductivity of the membrane. In the kinetic region, the performance is identical in air and HelOx with the kinetic resistance increasing after 30,000 cycles (Figure 9a). This increased kinetic resistance is due to both loss in electrocatalyst active surface area and leaching of Co, resulting in a reduced mass activity. At BOL, the kinetic resistance in both air and HelOx decreases with decreasing voltage (0.30 $\Omega{\cdot}cm^2$ at 0.2 A/cm^2), reaching a constant value of around 0.14 $\Omega{\cdot}cm^2$ at a current density $>$ 0.8 A/cm^2 consistent with Butler-Volmer kinetics. After 30,000 cycles this resistance increases to 0.35 $\Omega{\cdot}cm^2$ at 0.2 A/cm^2), reaching a constant value of around 0.18 $\Omega{\cdot}cm^2$ at a current density $>$ 0.8 A/cm^2. The mass transport component of the resistance develops near 1.0 A/cm^2 and increases with increasing current.

The resistance is significantly lower in HelOx than in air with the BOL mass transport resistance at 2 A/cm^2 of 0.14 $\Omega{\cdot}cm^2$ in air and only 0.04 $\Omega{\cdot}cm^2$ HelOx. It should be noted that the HFR (0.055 $\Omega{\cdot}cm^2$)

Table II. Rated power at three different operating temperatures for a nanofiber electrode MEA with a TKK PtCo/C cathode. Anode and cathode loadings were both 0.10 mg$_{Pt}$/cm^2. Feed gas flow rates: 500 sccm H_2, 2000 sccm air; Membrane: Nafion 211, Relative Humidity: 100%. Voltage was calculated from Equation 1. For a 90 kW stack and ambient temperature of 40°C.

Temperature (°C)	Pressure (kPa, absolute)	Potential (V)	Performance at Rated Power (mW/cm^2)
80	150	0.771	667
	150		784
95	200	0.674	906
	250		1,072
99	150	0.652	908

Table III. Mass activity and gas transport resistance (GTR) changes during the square wave accelerated stress test after either 15,000 or 30,000 voltage cycles with and without recovery measured at LANL.

	Nanofiber MEA Mass Activity (mA/mg_{Pt})	Nanofiber MEA GTR (s/m)	Spray MEA Mass activity (mA/mg_{Pt})	Spray MEA GTR (s/m)
BOL	270	35	N/A	N/A
BOL + 4 Recovery cycles	464	21	431	29
15k voltage cycles	236	35	121	41
15k voltage cycles + 4 Recovery cycles	496	28	231	37
30k voltage cycles	202	37	147	59
30k voltage cycles + 4 Recovery cycles	296	35	189	52

and kinetic resistance as determined from the impedance fits (0.14 $\Omega \cdot cm^2$) are identical in air and HelOx indicating that the difference observed in total resistance (0.1 $\Omega \cdot cm^2$) at 2.0 A/cm^2 can be attributed to the difference in mass transport resistance. At 2.0 A/cm^2, in addition to the kinetic resistance (in both air and HelOx) increasing to 0.18 $\Omega \cdot cm^2$, the mass transport resistance also increases with cycling and is 0.31 $\Omega \cdot cm^2$ and 0.08 $\Omega \cdot cm^2$ in air and HelOx respectively after 30,000 cycles. The amount of mass transport losses that can be recovered in HelOx is indicative of the pressure dependent transport term and still dominates the transport resistance ($\approx$ 70% of the total transport resistance). The pressure independent transport resistance (as evidenced by GTR) also increases with cycling but is only a small portion of the overall transport resistance as indicated by the HelOx measurements. Therefore, in addition to the increases in local O_2 transport resistance

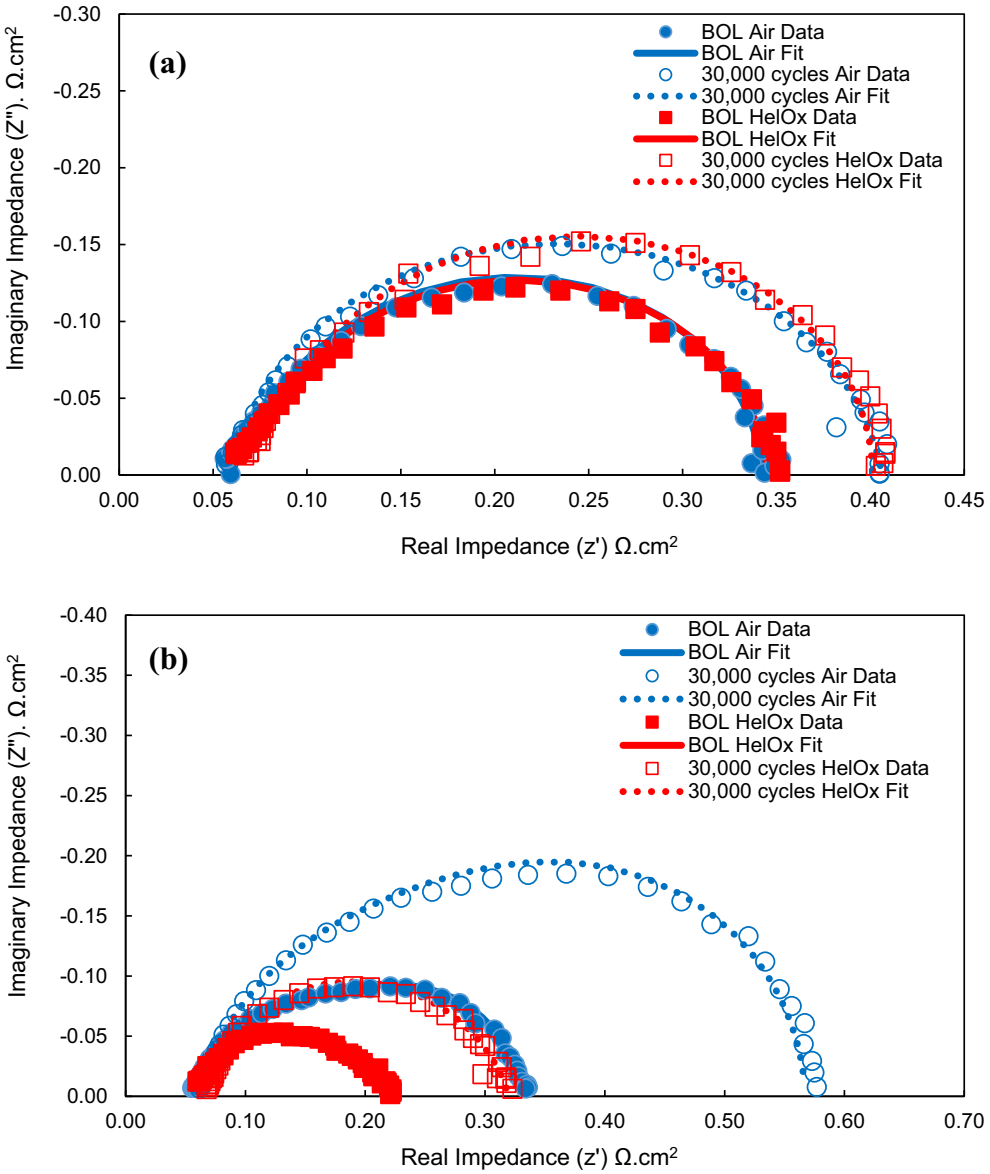

Figure 9. Electrochemical Impedance Spectra (EIS) of a 5 cm^2 nanofiber electrode MEAs with a PtCo/C cathode in air and HelOx before and after 30,000 cycles of catalyst AST. (a) 0.2 A/cm^2 and (b) 2.0A/cm^2. The equivalent circuit fit is given by the solid and lines; experimental data is shown by the markers.

caused by decreased catalyst surface area, molecular diffusion resistance also increases with catalyst cycling AST.

Conclusions

TKK PtCo/C was successfully electrospun into a nanofiber cathode mat with Nafion/PAA as the binder. Within a fiber, there was a uniform distribution of binder, catalyst particles, and void space. Intra-fiber porosity contributed 30% to the overall fiber surface area and the surface roughness of the fiber contributed another 20%. A nanofiber electrode MEA produced more power initially than a sprayed electrode MEA (e.g., a maximum power of 1,045 vs. 869 mW/cm^2 at 80°C and 200 kPa absolute pressure for anode and cathode catalyst loadings of 0.1 mg/cm^2 each) due to a higher mass activity and a lower gas transport resisitance (GTR), a consequence of the high inter-fiber and intra-fiber porosity of the nanofiber cathode with better (a more uniform) coating of binder on catalyst particles with little or no catalyst/binder agglomeration. The most significant benefit of the nanofiber electrode morphology was its durability; after a metal dissolution voltage cycling accelerated stress test, the nanofiber MEA lost only 8% of its initial maximum power, as compared to a 32% drop in maximum power for a sprayed electrode MEA. The high power and greatly improved durability of nanofiber cathode MEAs was associated with the unique submicon diameter nanofiber electrode morphology, where there is a uniform distribution of catalyst and binder (no agglomerates), intra and inter-fiber porosity, and short transport pathways in the radial fiber direction (where the latter two characteristics lower gas transfer resistance and facilitates water removal from catalyst sites). Smaller losses in ECSA and mass activity as well as a GTR that remained low and essentially unchanged after voltage cycling in nanofiber electrode MEAs are attributed to a greater amount of cobalt and Pt retention in PtCo metal nanoparticles and less particle growth.

Acknowledgments

This research is supported by the U.S. Department of Energy Fuel Cell Technologies Office, through the Fuel Cell Performance and Durability (FC-PAD) Consortium (Fuel Cells Program Manager: Dimitrios Papageoropoulos). The work at Vanderbilt University was funded under DOE contract No. DE-EE0007653.

ORCID

N. Macauley https://orcid.org/0000-0001-5602-0092
R. Mukundan https://orcid.org/0000-0002-5679-3930
K. More https://orcid.org/0000-0001-5223-9097
P. N. Pintauro https://orcid.org/0000-0001-5115-7276

References

1. P. Costamagna and S. Srinivasan, *J. Power Sources*, **102**, 242 (2001).
2. S. Litster and G. McLean, *J. Power Sources*, **130**, 61 (2004).
3. W. Zhang and P. N. Pintauro, *ChemSusChem*, **4**, 1753 (2011).
4. M. Brodt, R. Wycisk, and P. N. Pintauro, *J. Electrochem. Soc.*, **160**, F744 (2013).
5. M. Brodt, T. Han, N. Dale, E. Niangar, R. Wycisk, and P. Pintauro, *J. Electrochem. Soc.*, **162**, F84 (2015).
6. M. Brodt, R. Wycisk, N. Dale, and P. Pintauro, *J. Electrochem. Soc.*, **163**, F401 (2016).
7. M. Oezaslan, F. Hasché, and P. Strasser, *J. Phys. Chem. Lett.*, **4**, 3273 (2013).
8. C. Wang, N. M. Markovic, and V. R. Stamenkovic, *ACS Catal.*, **2**, 891 (2012).
9. E. Antolini, J. R. C. Salgado, M. J. Giz, and E. R. Gonzalez, *Int. J. Hydrogen Energy*, **30**, 1213 (2005).
10. S. Hidai, M. Kobayashi, H. Niwa, Y. Harada, M. Oshima, Y. Nakamori, and T. Aoki, *J. Power Sources*, **196**, 8340 (2011).
11. P. Yu, M. Pemberton, and P. Plasse, *J. Power Sources*, **144**, 11 (2005).
12. P. Gallo Stampino, C. Cristiani, G. Dotelli, L. Omati, L. Zampori, R. Pelosato, and M. Guilizzoni, *Catal. Today*, **147**, 30 (2009).
13. H. A. Gasteiger, S. S. Kocha, and B. Sompalli, *F. T. Appl. Catal. B Environ.*, **56**, 9 (2005).
14. K. R. Cooper, *Fuel Cell Mag. Scribner Assoc.*, **1**, 1 (2009).
15. D. R. Baker, D. A. Caulk, K. C. Neyerlin, and M. W. Murphy, *J. Electrochem. Soc.*, **156**, B991 (2009).
16. T. Mashio, A. Ohma, S. Yamamoto, and K. Shinohara, *ECS Trans.*, **11**, 529 (2007).
17. K. Sakai, K. Sato, T. Mashio, A. Ohma, K. Tamaguchi, and K. Shinohara, *ECS Trans.*, **25**, 1193 (2009).
18. Y. Fukuyama, T. Shiomi, T. Kotaka, and Y. Tabuchi, *Electrochim. Acta*, **117**, 367 (2014).
19. Y. Liu, M. W. Murphy, D. R. Baker, W. Gu, J. Jorne, and H. A. Gasteiger, *ECS Trans.*, **11**, 473 (2007).
20. R. Makharia, M. F. Mathias, and D. R. Baker, *J. Electrochem. Soc.*, **152**, A970 (2005).
21. P. M. Gomadam and J. W. Weidner, *Int. J. Energy Res.*, **29**, 1133 (2005).
22. Atsushi Ohma, Kazuhiko Shinohara, Akihiro Iiyama, Toshihiko Yoshida, and A. Daimaru, *ECS Trans.*, **41**, 775 (2011).
23. J. Zhang and L. Paine, *Patent Application Publication* (2011), US 2011/0195324 A1.
24. T. A. Greszler, D. Caulk, and P. Sinha, *J. Electrochem. Soc.*, **159**, F831 (2012).
25. A. Kongkanand and M. F. Mathias, *J. Phys. Chem. Lett.*, **7**, 1127 (2016).
26. A. Ohma, T. Mashio, K. Sato, H. Iden, Y. Ono, and K. Sakai, *Electrochim. Acta*, **56**, 10832 (2011).
27. R. Subbaraman, D. Strmcnik, A. P. Paulikas, V. R. Stamenkovic, and N. M. Markovic, *ChemPhysChem*, **11**, 2825 (2010).
28. K. Shinozaki, Y. Morimoto, B. S. Pivovar, and S. S. Kocha, *J. Power Sources*, **325**, 745 (2016).
29. F. T. Wagner, B. Lakshmanan, and M. F. Mathias, *J. Phys. Chem. Lett.*, **1**, 2204 (2010).
30. D. J. Myers, D. Myers, X. Wang, N. Kariuki, R. Subbaraman, R. Ahluwalia, and X. Wang, *U.S. DOE Hydrog. Fuel Cells Progr. Veh. Technol. Progr. Annu. Merit Rev.* (2011), Project ID, 1.
31. J. Marcinkoski, B. James, and C. Houchins, DOE Hydrog. Fuel Cells Progr. Rec. (2016), 1.
32. D. Papageorgopoulos, *Fuel Cells R&D Overview. Office of Energy Efficiency and Renewable Energy;U.S. DOE Hydrog. Fuel Cells Progr. Veh. Technol. Progr. Annu. Merit Rev.*, (2018).
33. S. Arisetty, X. Wang, R. K. Ahluwalia, R. Mukundan, R. Borup, J. Davey, D. Langlois, F. Gambini, O. Polevaya, and S. Blanchet, *J. Electrochem. Soc.*, **159**, B455 (2012).